Journal of Power Sources 194 (2009) 214–219

Contents lists available at ScienceDirect

Journal of Power Sources

journal homepage: www.elsevier.com/locate/jpowsour

In situ Van der Pauw measurements of the Ni/YSZ anode during exposure to syngas with phosphine contaminant

Oktay Demircan[a,*], Chunchuan Xu[b], John Zondlo[b], Harry O. Finklea[a,c]

[a] C. Eugene Bennett Department of Chemistry, West Virginia University, 217 Clark Hall Prospect Street, P.O. Box 6045, Morgantown, WV 26506, USA
[b] Department of Chemical Engineering, West Virginia University, Morgantown, WV 26506, USA
[c] National Energy Technology Laboratory-Institute for Advanced Energy Studies, US Department of Energy, Morgantown, WV 26505, USA

ARTICLE INFO

Article history:
Received 12 March 2009
Received in revised form 24 April 2009
Accepted 27 April 2009
Available online 3 May 2009

Keywords:
SOFC
Van der Pauw method
Syngas
Phosphine
Degradation
Anode resistivity

ABSTRACT

Solid oxide fuel cells (SOFCs) represent an option to provide a bridging technology for energy conversion (coal syngas) as well as a long-term technology (hydrogen from biomass). Whether the fuel is coal syngas or hydrogen from biomass, the effect of impurities on the performance of the anode is a vital question. The anode resistivity during SOFC operation with phosphine-contaminated syngas was studied using the *in situ* Van der Pauw method. Commercial anode-supported solid oxide fuel cells (Ni/YSZ composite anodes, YSZ electrolytes) were exposed to a synthetic coal syngas mixture (H_2, H_2O, CO, and CO_2) at a constant current and their performance evaluated periodically with electrochemical methods (cyclic voltammetry, impedance spectroscopy, and polarization curves). In one test, after 170 h of phosphine exposure, a significant degradation of cell performance (loss of cell voltage, increase of series resistance and increase of polarization resistance) was evident. The rate of voltage loss was 1.4 mV h^{-1}. The resistivity measurements on Ni/YSZ anode by the *in situ* Van der Pauw method showed that there were no significant changes in anode resistivity both under clean syngas and syngas with 10 ppm PH_3. XRD analysis suggested that Ni_5P_2 and P_2O_5 are two compounds accumulated on the anode. XPS studies provided support for the presence of two phosphorus phases with different oxidation states on the external anode surface. Phosphorus, in a positive oxidation state, was observed in the anode active layer. Based on these observations, the effect of 10 ppm phosphine impurity (or its reaction products with coal syngas) is assigned to the loss of performance of the Ni/YSZ active layer next to the electrolyte, and not to any changes in the thick Ni/YSZ support layer.

© 2009 Elsevier B.V. All rights reserved.

1. Introduction

The promise of coal syngas as a fuel for solid oxide fuel cells is mitigated by the effects of syngas contaminants on the Ni/YSZ anode [1–3]. Recent research has focused on the effect of volatile phosphorus species in syngas, especially phosphine (PH_3), on the long-term performance of the Ni/YSZ anode [4–6]. While debate exists on the chemical nature of compounds formed on the anode and current collector (phosphides or phosphates), there is general agreement on two points. Concentrations of phosphine in the ppm range in synthetic syngas mixtures cause immediate and irreversible loss of performance of the SOFC, and nickel metal migrates to the external surface of the anode and to cavities within the anode structure [7–9]. Nickel metal is known to migrate under methane reforming conditions on a Ni/YSZ powder [10].

Nickel migration could cause part of the performance loss through two mechanisms: (i) increased resistance of the current collection part of the Ni/YSZ anode (especially in an anode-supported cell) and (ii) loss of nickel (loss of TPB length) in the active layer of the anode. One approach to distinguishing these two mechanisms is to measure the anode resistivity, ρ, *in situ*, before, during and after exposure to syngas with phosphine contaminant. In a typical commercial anode-supported SOFC, the anode is constructed of a thick support layer and a thin active layer next to the electrolyte. Standard electrochemical methods for measuring the ohmic resistance of a SOFC cannot distinguish between ohmic losses in the two layers of the anode.

Van der Pauw (VdP) methods [11] are the standard for measuring sheet resistance without error due to contact resistance. Sheet resistance on the sample can be calculated by using Van der Pauw equation: $exp(-\pi R_{vertical}/R_S) + exp(-\pi R_{horizontal}/R_S) = 1$, R_S is the sheet resistance, $R_{vertical}$ and $R_{horizontal}$ are calculated from series of measurements by using four contacts on the anode surface (see below). In the Van der Pauw method, the contacts are located at the edges of the conducting surface. Two adjacent elec-

* Corresponding author. Tel.: +1 304 293 3435x6440; fax: +1 304 293 4904.
E-mail address: Oktay.Demircan@mail.wvu.edu (O. Demircan).

0378-7753/$ – see front matter © 2009 Elsevier B.V. All rights reserved.
doi:10.1016/j.jpowsour.2009.04.071

trodes are used to carry current and the two other electrodes are used to measure voltage. The slope of voltage–current scan is used to calculate resistance for each combination of electrode connections. When four contacts on the sample are symmetrically located with respect to the surface and the composition on the sample is homogenous, both $R_{vertical}$ and $R_{horizontal}$ should be very close. R_S is calculated from VdP equation and is multiplied by the thickness of the sample to obtain the resistivity, ρ.

Jiang and Chan reviewed the effects of nickel content and microstructure on Ni/YSZ composites [12]. Few *in situ* conductivity measurements have been reported for SOFC electrodes during operation [13,14]. A typical Ni/YSZ composite structure with a thickness of 0.6 mm has a resistivity of 1700–2500 μΩ cm at 800 °C [13]. We report here *in situ* measurements of sheet resistance, R_S, and resistivity of the anode of a commercial SOFC during prolonged exposure to wet hydrogen, then clean syngas, and then syngas with 10 ppm phosphine. The effect of the prolonged exposure of the anode to phosphine with current flow was investigated using extensive post-mortem analyses.

2. Experimental methods

A commercial SOFC obtained from MSRI was mounted as shown in Fig. 1. The four Au leads on the anode surface and the Au gauze on cathode surface appear in Fig. 1a and c, respectively. The anode and cathode sides after mounting in alumina flanges are shown in Fig. 1b and d, respectively. Four 2 mm × 2 mm contacts were formed using flattened gold wire and gold paste in a square array. The contacts lie inside of the mica gaskets and alumina flange that seal the anode side. The Van der Pauw equation is based on the assumption that four point contacts are made at the very edge of a conducting sheet [11]. Consequently, the sheet resistances obtained by this configuration are not accurate, but changes in the sheet resistance are measurable. The cathode current collector is gold mesh with gold paste on the periphery. A current-carrying wire and a voltage-sensing wire were connected to the gold mesh.

Details on the furnace and gas handling system are given in the previous paper [9]. The furnace temperature was ramped to 800 °C over 7 h while exposing the anode to a dry H_2 (30 sccm)-N_2 (200 sccm) gas mixture and the cathode to air (200 sccm). The assembly was kept at 800 °C overnight to make sure NiO completely reduced to Ni. Next, the nitrogen flow was cut while the flow rate of H_2 was increased to 200 sccm and water vapor at 3% concentration was provided by a humidifier. The flow rate of air to the cathode was increased to 300 sccm. The cell was loaded with 0.5 A constant current while monitoring voltage for 1 day. All electrochemical measurements were acquired using a Solartron SI 1287 potentiostat. Impedance spectra were acquired using a Solartron SI 1260 impedance/gain-phase analyzer with AC amplitude of 20 mV at frequencies ranging from 100 kHz to 0.1 Hz. Cell polarization curves, VdP measurements and impedance spectra were completed everyday. The SOFC was exposed to the following sequence of fuel mixtures: (i) 194 sccm (97%) H_2 with 6 sccm (3%) water vapor for 70 h; (ii) 60 sccm (30%) H_2 plus 88 sccm (44%) N_2 with 52 sccm (26%) water vapor to mimic syngas mixture without CO/CO_2 for 2.5 h; (iii) syngas (60 sscm (30%) H_2, 52 sccm (26%) H_2O, 46 sccm (23%) CO, and 42 sccm (21%) CO_2) for 170 h; (iv) syngas with 10 ppm PH_3 for 170 h. The SOFC was cooled to room temperature in 5 h with the anode exposed to 20 sccm (10%) H_2 with 180 sccm (90%) N_2 to minimize air oxidation.

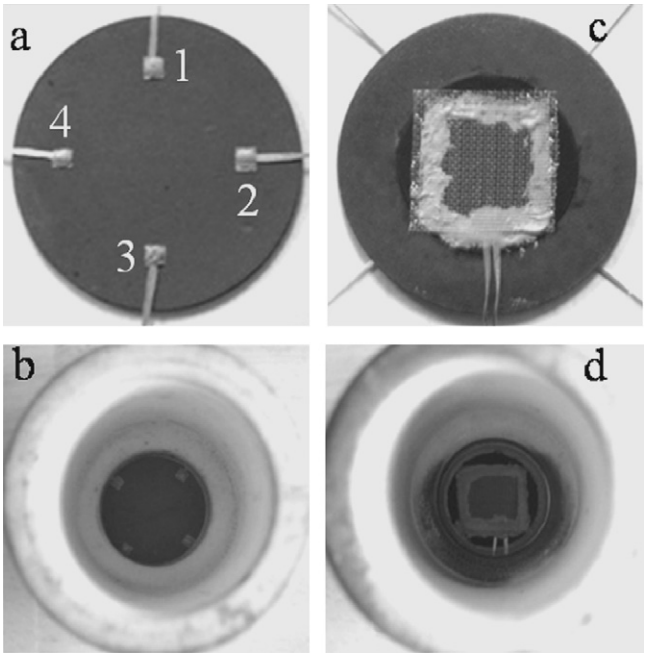

Fig. 1. Experimental setup: (a) four Au leads on anode surface; (b) anode side after putting in the alumina flange; (c) Au grid on cathode surface; (d) cathode side after putting in the alumina flange.

For convenience, the four contacts to the anode are labeled 1 through 4 clockwise as seen in Fig. 1a. The Solartron potentiostat provides four connections to the SOFC, the current-carrying working (WE) and counter (CE) leads, and the voltage-sensing reference leads (RE1 and RE2). To load the cell, to measure the cell performance and to collect electrochemical impedance spectra (EIS) on the cell, wires 1 and 3 were connected to the WE lead and wires 2 and 4 were connected to the RE2 lead on the potentiostat. The two cathode leads were connected to the CE and RE1 leads on the potentiostat. To acquire Van der Pauw (VdP) resistance measurements, the four leads on anode side were connected to the Solartron potentiostat so that two adjacent contacts carried the current and the other two adjacent contacts measured a voltage. For example, the first measurement has the following connections: 1-RE1, 2-RE2, 3-WE, 4-CE. The connections to the potentiostat were rotated (1234, 2341, 3412, and 4123) and the VdP measurement repeated. 1234 and 3412 yield $R_{vertical}$ and 2341 and 4123 yield $R_{horizontal}$. The VdP measurement consisted of a current scan from 0 to +0.5 and then −0.5 to 0 A Because of the low sheet resistance of the reduced Ni/YSZ anode, voltage measurements did not exceed 2 mV. Noise level in these scans was less than 5 μV.

The surface and cross-section analyses of the cell anode were studied with a Hitachi S-4700 SEM. XRD (Panalytical X'Pert PM-3040 PRO) and XPS (PHI 5000 VerasProbe XPS Microprobe) were employed to analyze the composition of the anode.

3. Results and discussion

The long-term performance data of the cell under 0.5 A constant current load at 800 °C is displayed in Fig. 2. During the first 3 days, the cell voltage under H_2 with 3% water is constant at 0.80 V. When the water content is increased to 26% and H_2 content decreased to 30% (balanced with 44% N_2), the voltage drops to 0.72 V in 30 min, in agreement with Nernst equation. During the 7 days of operation under syngas, the cell voltage fluctuates around 0.7 ± 0.02 V. However, as soon as 10 ppm PH_3 is added to the syngas mixture, the cell voltage under load starts decreasing at the rate of 1.4 mV h^{-1}. After 7 days (170 h) operation with 10 ppm PH_3, the voltage decreased to 0.47 V (∼33% overall degradation). Marina et al. [6] used 1–5 ppm PH_3 as the impurity in syngas mixtures and observed degradation rates of 1.0–1.4 mV h^{-1}.

The polarization curves for different fuel compositions are illustrated in Fig. 3. As summarized in Table 1, 97% H_2 with 3% water has the best performance (highest voltage at 0.25 A cm^{-2}, power

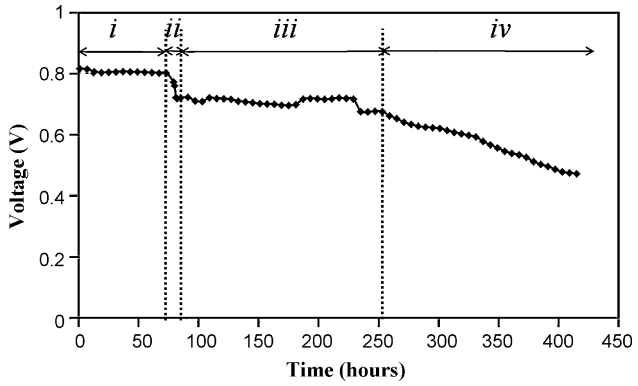

Fig. 2. Long-term performance as voltage data under 0.5 A (0.25 A cm^{-2}) constant current load at 800 °C: (i) 97% H_2 with 3% water; (ii) 30% H_2 with 26% water and 44% N_2; (iii) syngas; (iv) syngas with 10 ppm PH_3.

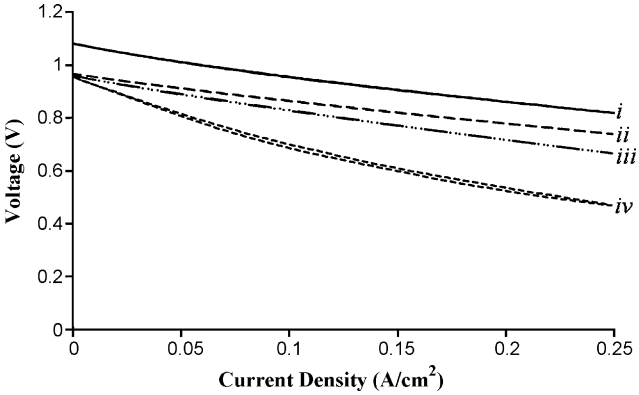

Fig. 3. Performance curves for different fuel compositions at 800 °C: (i) 97% H_2 with 3% water; (ii) 30% H_2 with 26% water and 44% N_2; (iii) syngas; (iv) syngas with 10 ppm PH_3.

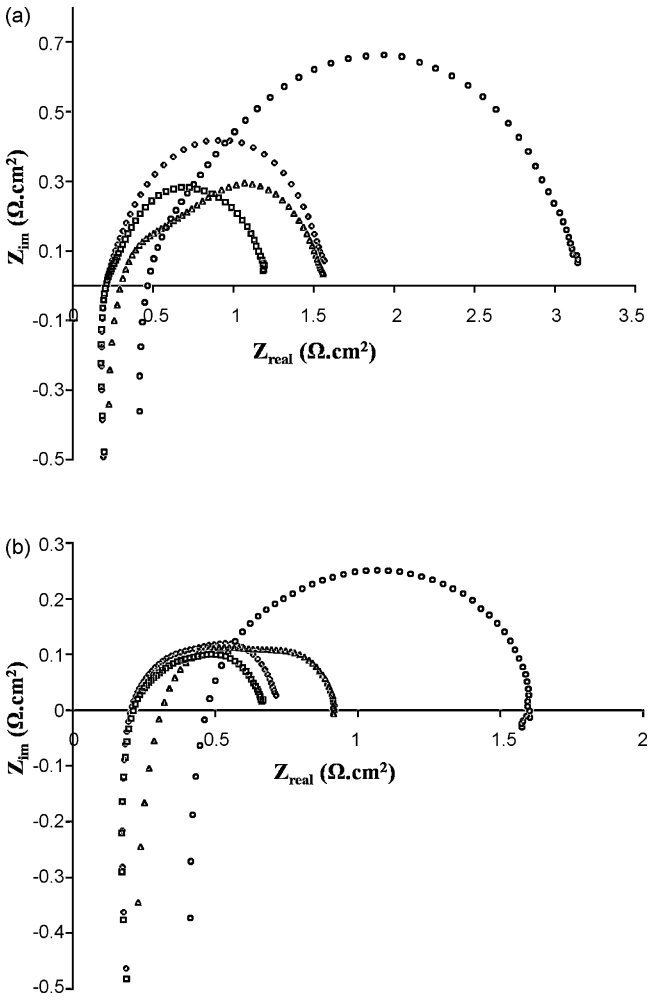

Fig. 4. EIS data for different fuel compositions at 800 °C: (a) at OCV and (b) at 400 mV overpotential ((◊) 97% H_2 with 3% water; (□) 30% H_2 with 26% water and 44% N_2; (△) syngas; and (○) syngas with 10 ppm PH_3).

density at 0.2 W cm^{-2}) over 3 days. When hydrogen is diluted with nitrogen and water vapor, power density decreases by 10%. Syngas performance in comparison of current at 0.7 V potential is ~10% less than H_2 with high water content, despite the potential presence of extra hydrogen due to the water gas shift reaction with CO and steam. Over 7 days of operation under syngas with 10 ppm PH_3, current density decreases 30% with respect to initial syngas current density at 0.7 V potential.

The open circuit voltage (OCV) values are also compared in Table 1. The OCV value for H_2 with 3% water is around 1.08 V, which is 20 mV lower than OCV predicted by the Nernst equation (1.10 V). This discrepancy is commonly attributed to small leaks in the electrolyte and in the anode seals. When more water is added to the fuel stream with a lower H_2 concentration, the OCV decreases to ~0.97 V. The predicted Nernst OCV for 30% H_2 + 26% H_2O + 21% O_2 is 0.948 V. The expected OCV for 23% CO + 21% CO_2 + 21% O_2 is 0.949 V, implying near equilibrium for the water gas shift reaction under OCV conditions. The measured OCV of 0.97 V suggests that the ratio of hydrogen to water is higher than expected. In half-cells with two half-reactions, the mixed potential tends to be dominated by the half-reaction with faster kinetics, in this case the H_2/H_2O half-reaction [15]. The OCV value of the syngas mixture is initially close to 0.97 V for 2–3 days; however, it drops to ~0.96 V over 7 days. The initial OCV of syngas with 10 ppm PH_3 is very close to the OCV of the pure syngas mixture; however, it also drops from ~0.96 V to ~0.95 V over 7 days. The cause for the drop in OCV implies either a change in the leak rate with time, or changes in the H_2/H_2O ratio in the anode gas stream with time.

Electrochemical impedance spectroscopy (EIS) data for different fuel compositions at OCV and 400 mV overpotential are shown in Fig. 4a and b. Series and polarization resistances from the impedance plots are summarized in Fig. 5. R_{ohmic} is the ohmic resistance which is acquired from the intercept on the high frequency side of the real impedance; R_p is the polarization resistance which is the difference between the low frequency intercept and R_{ohmic}. As shown in Fig. 4, the ohmic resistance, R_{ohmic}, values are virtually the same between OCV and 400 mV overpotential under the same conditions; hence, this is the reason to show one type of R_{ohmic} for OCV and 400 mV in Fig. 5. Similarly, R_{ohmic} values of

Table 1
Summary of the performance for different fuel mixtures at 800 °C.

	H_2 with 3% water	H_2 with 26% water	Syngas after 170 h	Syngas + PH_3 after 170 h
Open circuit voltage (V)	1.08	0.97	0.96	0.95
Voltage (V) at 0.5 A constant current	0.80	0.72	0.70	0.47
Power density (W cm^{-2}) at 0.5 V cell voltage	0.20	0.18	0.17	0.12

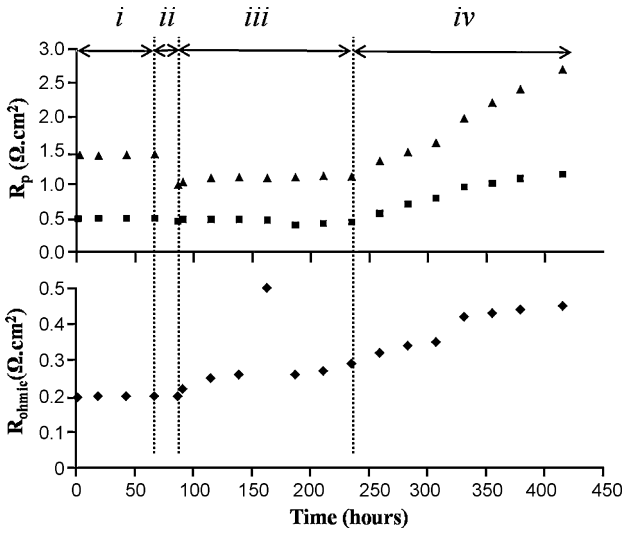

Fig. 5. EIS data summary for different fuel compositions: (i) 97% H_2 with 3% water; (ii) 30% H_2 with 26% water and 44% N_2; (iii) syngas; (iv) syngas with 10 ppm PH_3 ((♦) R_{ohmic}; (■) R_p at 400 mV overpotential; (▲) R_p at OCV).

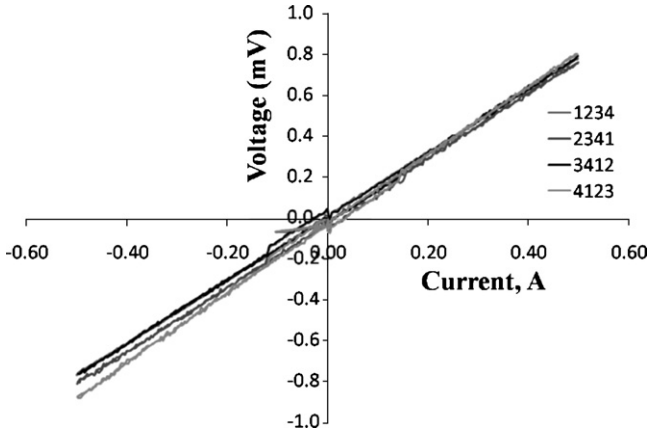

Fig. 6. VdP data as a current–voltage scan for H_2 with 3% water. All four combinations, 1234, 2341, 3412, and 4123, are shown and are virtually identical.

0.2 Ω cm² do not change between two different water contents. R_p measured at OCV decreases with a higher water-to-hydrogen ratio in the fuel stream [16,17]. We have observed that R_{ohmic} and R_p values increase slightly over 2–3 days under syngas mixture, but these values become stable afterwards. One data point at 0.5 Ω cm² at around 170 h is believed to be an outlier in this data set. R_{ohmic} and R_p values increase when 10 ppm PH_3 is added to the fuel stream. The resistance changes during PH_3 exposure are noticeably greater than the changes during the exposure to clean syngas. These changes account for the degradation in the cell performance. Since R_{ohmic} values increase during exposure to the phosphine, the question arises as to the location of the increase in the series resistance. To answer this question, *in situ* Van der Pauw measurements are performed [11].

VdP measurements and slopes (as resistance) for 97% H_2 with 3% water vapor are shown in Fig. 6. All of such data plots are linear with zero intercepts, consistent with pure ohmic behavior and no distortion due to local differences in the potentials across the Ni/YSZ composite. These resistances from the slopes from all four scans are inserted into the Van der Pauw to obtain the sheet resistance. The resistivity, ρ, is calculated from the sheet resistance multiplied by the thickness of anode, 0.080 cm, which measured by scanning electron microscope (SEM). Resistivity values (Table 2) range in between 575 and 610 μΩ cm. The uncertainty of each value is estimated to be 5%, and the relative standard deviation of all values given in parenthesis (Table 2) is in 0.5–2% range, so the resistivity is constant within the uncertainty of the measurements. The average value is 598 (±13) μΩ cm. This resistivity value is consistent with a prior report for an anode-supported cell [13]. To understand the discrepancy between this observation and the increase in the ohmic resistance during phosphine exposure, a comprehensive post-mortem analysis of the anode was performed. The results are described below.

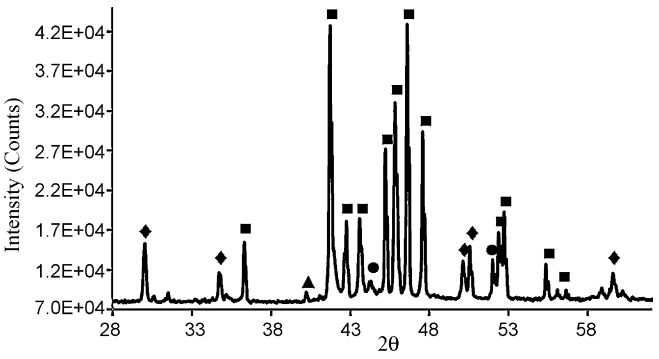

Fig. 7. XRD analysis on Ni–YSZ anode-supported cell surface after 170 h of syngas with 10 ppm PH_3 exposure ((♦) YSZ; (■) Ni_5P_2; (▲) P_2O_5; (●) Ni).

The XRD analysis of the PH_3-poisoned Ni–YSZ anode surface is illustrated in Fig. 7. YSZ, Ni_5P_2, P_2O_5, and Ni peaks are labeled in XRD spectrum. The XRD spectrum confirms that $Ni_3(PO_4)_2$ is not produced on the surface [18,19]. The five YSZ peaks at 30.00°, 34.69°, 50.10°, 50.30° and 59.57° appear clearly in the XRD spectrum [20]. Although Ni_5P_2, Ni_3P, Ni_8P_3 and $Ni_{12}P_5$ peaks can overlap in the XRD spectrum, the 45.81° and 47.56° peaks are consistent with Ni_5P_2 [21]. This phase has been reported in a previous paper [9]. Trembly [2] and Xu et al. [9] show that Ni_5P_2 would be the main product according to thermodynamic equilibrium calculations for the fuel combination of 2 ppm and 10 ppm PH_3 in syngas, respectively. Recent studies conducted by Marina et al. [6] on a Ni–YSZ anode-supported cell exposed to 2 ppm PH_3 in syngas report the formation of Ni_3P on both the anode surface and the metallic Ni current collector. The weak peak at 40.17° is attributed to P_2O_5, which is also a possible product under SOFC operation conditions [22]. Ni peaks appear at 44.16° and 51.98° but no NiO peaks are observed.

The SOFC was fractured and different points for XPS analysis are displayed in Fig. 8. The sample points are labeled as follows: (1) black-brown spot on the anode surface which is co-linear with the gas inlet tube; (2) shiny grey spot on the anode surface; (3) grey spot under the mica gasket; (4) on the cross-section of the cell near to active anode layer (the XPS beam size is adjusted to 20 μm diameter to focus on only the active anode region).

The first point on the brown spot is analyzed with XPS (Fig. 9). The Y and Zr peaks are absent, indicating that a coating lies over

Table 2
The resistivity, ρ, analysis using VdP measurements. Standard deviations are 1–2% and given as ± after the data.

	H_2 with 3% water	H_2 with 26% water	Syngas after 24 h	Syngas after 96 h	Syngas after 170 h	Syngas + PH_3 after 24 h	Syngas + PH_3 after 96 h	Syngas + PH_3 after 170 h
Resistivity (μΩ cm)	575 ± 3	585 ± 4	588 ± 3	608 ± 8	610 ± 3	606 ± 7	605 ± 6	608 ± 3

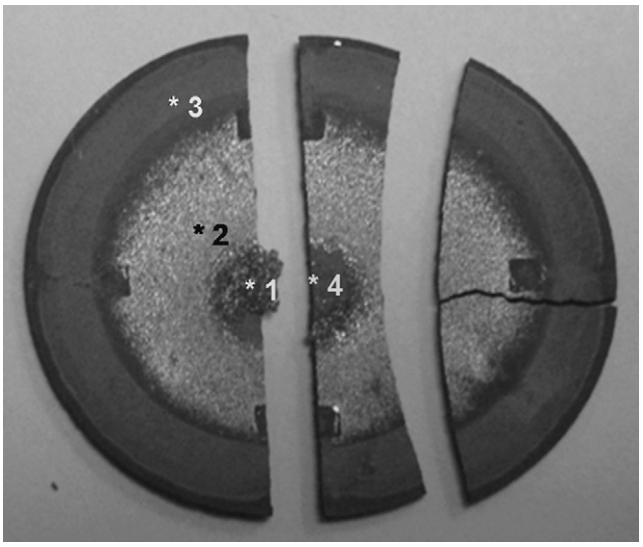

Fig. 8. XPS sample places: (1) black-brown spot on anode surface; (2) shiny grey spot on anode surface; (3) grey spot under mica gasket; (4) on the cross-section of the cell near to in the active anode layer (adjusted spot size is 20 μm).

the YSZ/Ni composite. Fe 2p3 and P 2p binding energy region scans are shown in the inset. Fe^{2+} [23] on the XPS spectrum is observed on the anode surface. We speculate that the iron arises from volatile iron carbonyls from the CO gas tank or the gas transfer lines. The inset showing the P 2p detail scan clearly indicates the presence of one type of P with a binding energy around 134.2 eV. This binding energy value is consistent for phosphorus with a +5 oxidation state, for which phosphates and P_2O_5 compounds are possibilities [23,24]. Since no phosphate compounds are observed in XRD analysis, we hypothesize that P_2O_5 is the main reason of this peak.

As clearly seen in Fig. 8, there is a shiny metallic region on the anode surface exposed to the fuel stream, in contrast to the dull grey region underneath the mica gasket. The XPS survey scan of the second point is shown in Fig. 10. Again, the Y and Zr peaks are absent, indicating the presence of a new layer of material on the exposed anode surface. No Fe 2p3 peak is observed in this shiny metallic area. The Ni 2p3 region scan (inset) shows a peak at 852.8 eV, which is the signature peak for nickel metal [23,25] and also for Ni–P alloys [26]. No peak for NiO at 854 eV is observed. The P 2p binding energy region scan (inset) shows two different P 2p peaks, a doublet at 130.4 eV and a single peak at 134.2 eV. The peaks at 130.4 eV are

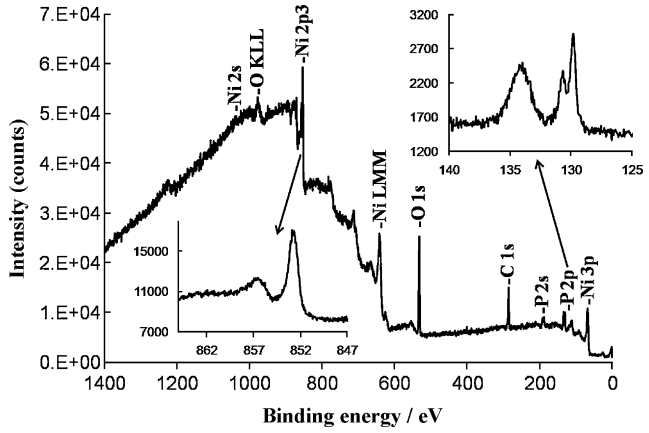

Fig. 10. XPS survey spectrum on shiny grey area (2nd point) spot; inset: the left inset is detail scan on Ni 2p3 range and the right inset is detail scan in P 2p range.

attributed to phosphorus with either a zero or negative oxidation state [27,28]. In this case, the most likely phosphorus compound is Ni_5P_2, in agreement with the XRD analysis. The other peak at 134.2 eV is assigned to P_2O_5 (+5 oxidation state phosphorus form).

The XPS spectra of the third point under the mica gasket are shown in Fig. 11. Ni 2p3 and Si 2p scans are also displayed in the inset of Fig. 11. All of the Si, Y, Zr and Ni peaks are clearly seen in the survey scan. The Ni 2p3 binding energy region scan shows the Ni peak at 854 eV consistent with NiO. The detail scan on the Si 2p region shows a peak at 104.0 eV [23]. Si can be easily transferred at this temperature range and the only known source of Si is the mica gasket. No P peaks are detected, which is expected because the mica gasket seals against the fuel stream.

The most useful XPS analysis is a 20 μm spot scan on the cross-section of the anode active region, in order to address the issues about the phosphorus migration to the interlayer between anode and electrolyte (Fig. 12). C, O, Ni, Fe, Y, Zr, and P detail scans were also obtained. Only the Ni and P scans are displayed in the insets of Fig. 12. At this interlayer between the anode and electrolyte, Fe is not observed, which indicates no Fe migration through the Ni–YSZ anode support. However, the detail scan over the P 2p binding energy range shows a peak at 134 eV. As explained above, this peak is attributed to P_2O_5 in this interlayer. Hence, phosphorus migration through the anode support layer is confirmed. There is no evidence for phosphide (e.g., Ni_5P_2) in the P 2p binding energy region. However, a more detailed and longer scan would be needed to observe other types of phosphorus compounds.

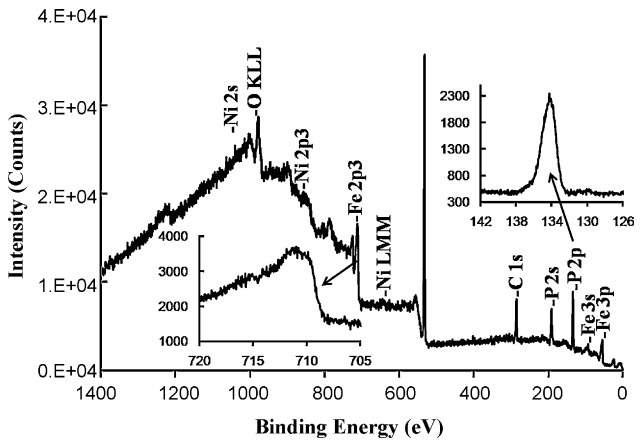

Fig. 9. XPS survey spectrum on black-brown spot (1st point); inset: the left inset is detail scan on Fe 2p3 range and the right inset is detail scan in P 2p range.

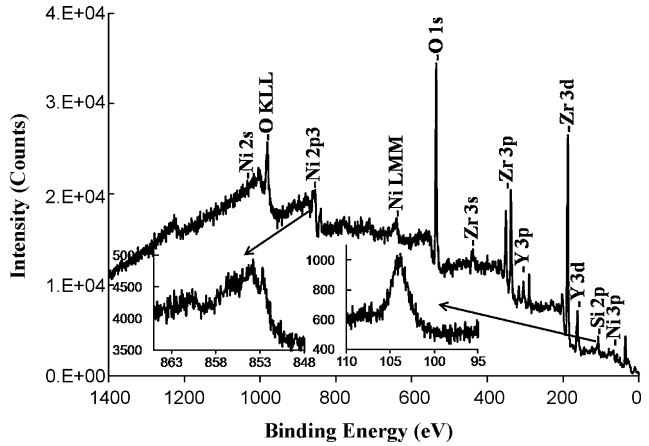

Fig. 11. XPS survey spectrum under mica area (3rd point); inset: the left inset is detail scan on Ni 2p3 range and the right inset is detail scan in Si 2p range.

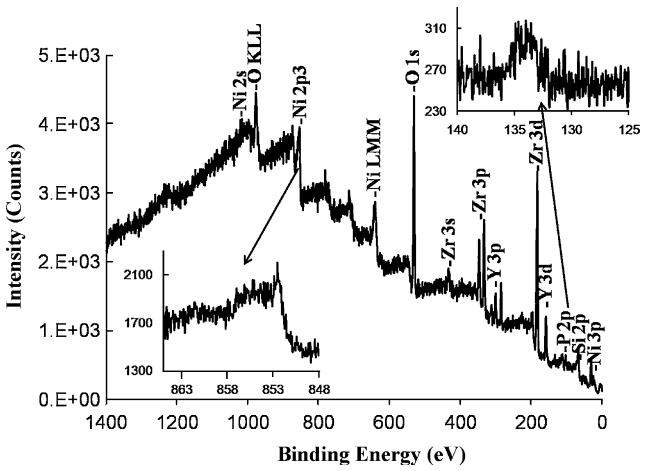

Fig. 12. XPS survey spectrum on the cross-section of the cell near to active anode layer (4th point); inset: the left inset is detail scan on Ni 2p3 range and the right inset is detail scan in P 2p range.

4. Summary

It is helpful to summarize all of the observations. SOFC performance degrades immediately and continuously upon addition of 10 ppm of phosphine gas to a syngas mixture. The degradation coincides with an increase in the ohmic resistance and an increase in the polarization resistance of the SOFC both at OCV and at 400 mV overpotential. However, Van der Pauw measurements show no significant change in the resistivity of the anode over the entire measurement period. Post-mortem XRD analysis indicates the presence of nickel phosphide and P_2O_5 phases. XPS analyses in various areas on the anode external surface show the presence of two coatings that cover up the YSZ/Ni composite layer. Directly beneath the anode gas inlet is a dark spot which contains iron in the +2 oxidation state and phosphorus in the +5 oxidation state. The rest of the exposed anode has a metallic luster. XPS analysis of this layer indicates the presence of Ni metal or Ni alloy and two forms of phosphorus, both P (+5) and P either in the (0) or (−3) oxidation state. Underneath the mica gaskets, XPS detects the presence of Y and Zr phases, and a silicon impurity attributed to contamination by the gasket. A spot analysis of the active layer of the anode detects phosphorus in the +5 oxidation state.

In our previous paper [9], we conclude that metallic nickel migrates to the surface of the anode and the void spaces inside the anode structure. The surface layer of nickel accounts for the absence of Y and Zr peaks in the XPS spectrum of the exposed anode surface. The XPS analysis suggests that the surface of the external nickel layer may contain both nickel phosphide and phosphorus oxide phases. The presence of a surface layer of nickel may account for the absence of a change in the anode resistivity, even though nickel is migrating out of the percolation network in the Ni/YSZ support. However, the VdP measurement is likely to be controlled by the 800 μm thick support layer of the anode-supported SOFC. Consequently, we tentatively assign the increase in ohmic resistance (from EIS measurements) to loss of nickel from the active layer of the anode. This loss would also reduce the TPB length and lead to an increase in the polarization resistance. Similarly, the presence of phosphorus oxide in the active layer suggests that increases in polarization resistance can be also attributed to poisoning of the nickel surface.

5. Conclusion

The effect of 10 ppm PH_3 as an impurity in a syngas mixture has been studied [1–6]. After addition of 10 ppm PH_3 the cell voltage at constant current linearly degrades with the rate of 1.4 mV h^{-1}, in excellent agreement with published results [6]. *In situ* Van der Pauw measurements are used to track the resistivity of the Ni–YSZ anode during exposure to various fuel mixtures at 800 °C. These *in situ* VdP measurements reveal that resistivity values under different fuel compositions, even with 10 ppm PH_3 impurity in syngas, are constant with an uncertainty of ∼5%. Electrochemical impedance spectroscopy (EIS) measurements indicate that an increase in both the ohmic resistance, R_{ohmic} and polarization resistance, R_p are caused by PH_3 exposure. Analyses using XRD and XPS suggest that Ni_5P_2 and P_2O_5 phases form on the anode surface. XPS data are also show that Fe appears on the anode surface. The iron is attributed to iron carbonyls in the syngas, possible from the CO tank and steel tube transfer lines. Both Ni migration out of the active layer and the formation of P_2O_5 phase in the anode active layer are stated as the main reasons of the cell performance degradation.

Acknowledgements

This study is performed under US DOE-EPSCoR Program. NETL (National Energy Technology Laboratory), US DOE Office of Basic Energy Sciences, WV State EPSCoR Office and West Virginia University are combined sponsors under grant number of DE-FG02-06ER46299. In this project Dr. Tim Fitzsimmons is the DOE Technical Monitor. Dr. Richard A. Bajura is the Administrative Manager and Dr. Ismail Celik is the Technical Manager and Principal Investigator. The authors would like to express gratitude to Dr. Andy Woodworth, Dr. Liviu Magean, and Mrs. Andrina MacLeod for XPS, SEM, EDS and XRD data.

References

[1] F.N. Cayan, M.J. Zhi, S.R. Pakalapati, I. Celik, N.Q. Wu, R. Gemmen, J. Power Sources 185 (2008) 595–602.
[2] J.P. Trembly, Investigation into the effects of trace coal syngas species on the performance of solid oxide fuel cell anodes, Ph.D. Dissertation, 2007.
[3] J.P. Trembly, R. Gemmen, D.J. Bayless, Proceedings of the 5th International Fuel Cell Science, Engineering and Technology Conference, New York, NY, 2007.
[4] J.P. Trembly, R.S. Gemmen, D.J. Bayless, J. Power Sources 163 (2007) 986–996.
[5] L.R. Pederson, O.A. Marina, X.D. Zhou, Y.S. Chou, G.W. Coffey, V.9 SECA Coal-Based Systems Core Research. V. Advanced Research. DOE FY 2007 Annual Report, 2007.
[6] O.A. Marina, L.R. Pederson, D.J. Edwards, C.W. Coyle, J. Templeton, M. Engelhard, Z. Zhu, Proceedings of the 8th Annual SECA Workshop, San Antonio, TX, 2007.
[7] F. Zhao, A.V. Virkar, J. Power Sources 141 (2005) 79–95.
[8] M.J. Zhi, X.Q. Chen, H. Finklea, I. Celik, N.Q.Q. Wu, J. Power Sources 183 (2008) 485–490.
[9] C. Xu, J.W. Zondlo, H.O. Finklea, O. Demircan, M. Gong, X. Liu, J. Power Sources, accepted for publication.
[10] D.L. King, J.J. Strohm, X.Q. Wang, H.S. Roh, C.M. Wang, Y.H. Chin, Y. Wang, Y.B. Lin, R. Rozmiarek, P. Singh, J. Catal. 258 (2008) 356–365.
[11] L.J. Van der Pauw, Philips Res. Rep. 13 (1958) 1–9.
[12] S.P. Jiang, S.H. Chan, J. Mater. Sci. 39 (2004) 4405–4439.
[13] S.P. Jiang, J.G. Love, L. Apateanu, Solid State Ionics 160 (2003) 15–26.
[14] S. Charojrochkul, K.L. Choy, B.C.H. Steele, Solid State Ionics 121 (1999) 107–113.
[15] O. Costa-Nunes, R.J. Gorte, J.M. Vohs, J. Power Sources 141 (2005) 241–249.
[16] A. Bieberle, L.P. Meier, L.J. Gauckler, J. Electrochem. Soc. 148 (2001) A646–A656.
[17] S.P. Jiang, Y. Ramprakash, Solid State Ionics 122 (1999) 211–222.
[18] C. Calvo, R. Faggiani, Can. J. Chem. 53 (1975) 1516.
[19] H. Onoda, D. Mori, K. Kojima, H. Nariai, Inorg. Mater. 41 (2005) 1089–1096.
[20] M.B. Pomfret, C. Stoltz, B. Varughese, R.A. Walker, Anal. Chem. 77 (2005) 1791–1795.
[21] G.S. Saini, L.D. Calvert, J.B. Taylor, Can. J. Chem. 42 (1964) 1511–1517.
[22] J.D. Hanawalt, H.W. Rinn, L.K. Frevel, Ind. Eng. Chem., Anal. Ed. 10 (1938) 457–475.
[23] J.F. Moulder, W.F. Stickle, P.E. Sobol, K.D. Bomben, Handbook of X-ray Photoelectron Spectroscopy, Physical Electronics, Eden Prairie, MN, 1995.
[24] R. Franke, T. Chasse, P. Streubel, A. Meisel, J. Electron Spectrosc. Relat. Phenom. 56 (1991) 381–388.
[25] A.B. Mandale, S. Badrinarayanan, S.K. Date, A.P.B. Sinha, J. Electron Spectrosc. Relat. Phenom. 33 (1984) 61–72.
[26] M.G. Thube, S.K. Kulkarni, D. Huerta, A.S. Nigavekar, Phys. Rev. B 34 (1986) 6874–6879.
[27] B. Elsener, M. Crobu, M.A. Scorciapino, A. Rossi, J. Appl. Electrochem. 38 (2008) 1053–1060.
[28] R. Franke, Spectrosc. Acta Pt. A-Mol. Biomol. Spectrosc. 53 (1997) 933–941.